IOP Publishing Measurement Science and Technology
Meas. Sci. Technol. **34** (2023) 015114 (17pp) https://doi.org/10.1088/1361-6501/ac8dae

A transfer-learning fault diagnosis method considering nearest neighbor feature constraints

Mengjie Zeng[1], Shunming Li[1,2,*], Ranran Li[1], Jiacheng Li[3], Kun Xu[1] and Xianglian Li[1]

[1] College of Energy and Power Engineering, Nanjing University of Aeronautics and Astronautics, Nanjing 210016, People's Republic of China
[2] School of Automotive Engineering, Nantong Institute of Technology, Nantong 226002, People's Republic of China
[3] Unmanned System Research Institute, Northwestern Polytechnical University, Xian 710072, People's Republic of China

E-mail: smli@nuaa.edu.cn

Received 9 June 2022, revised 29 July 2022
Accepted for publication 30 August 2022
Published 21 October 2022

Abstract

Aiming at the problem of low diagnostic accuracy of fault diagnosis models due to changes in actual operating conditions, a novel fault diagnosis method based on transfer learning considering nearest neighbor feature constraints is proposed. First, nearest neighbor samples are considered to measure data features. In addition, a nearest neighbor feature constraint strategy is designed to improve the feature extraction performance of the network. Second, a multiple-alignment strategy of nearest neighbor samples is proposed to enhance the domain adaptation performance of the network model utilizing multiple alignments. Then, a loss function dynamic weight strategy is used to improve the convergence of the loss function during model training. Finally, the experimental verification is carried out on the public data set of the Western Reserve University and the private data set. The experimental results show that the proposed method exhibits superior transfer performance with reliability and stability compared to the existing methods.

Keywords: domain adaptation, nearest neighbor, autoencoder, dynamic weights, distance constraint

(Some figures may appear in colour only in the online journal)

1. Introduction

Since the state of rotating mechanical parts has an important impact on the safe operation of machinery, it is necessary to conduct fault diagnosis research on components [1]. In recent years, with further research on deep learning, data-driven intelligent diagnosis algorithms have developed rapidly [2, 3]. Their main advantage is that they can perform intelligent feature extraction on data from massive data [4, 5]. Compared to common neural network algorithms, the superiority of autoencoder (AE) in feature reconstruction is not negligible [6–9]. The structure of an AE consists of an encoder and a decoder, which means that it can easily reconstruct the data for dimensionality reduction. Therefore, AE is widely used as a feature extractor in fault diagnosis applications.

Although many intelligent diagnostic algorithms have been able to achieve excellent diagnostic performance, most of them are based on the assumption that the training set and testing set are located in the same distribution, which brings limitations to conventional data-driven algorithms [10–12]. To address the problem of inconsistent domain distributions, domain adaptation research has been been given priority. Domain adaptation can adapt to or reduce the distribution

* Author to whom any correspondence should be addressed.

difference between the source domain and the target domain through fine-tuning of model weights or distribution alignment, to achieve reliable fault diagnosis under variable operating conditions [13, 14]. Azamfar *et al* [15] proposed a novel 1D deep convolutional transfer-learning method capable of learning high-dimensional domain-invariant features from a labeled training data set and performing diagnostic tasks on a domain-shifted unlabeled test data set. Wang *et al* [16] constructed an originality deep transfer-learning model called a multi-scale deep intra-class adaptation network to overcome the problem of different domain distributions. A novel deep structure based on a novel sparse denoising autoencoder was constructed by Xia *et al* and pre-trained with source domain conditional data generated from digital twins [17]. The above methods have achieved fault diagnosis based on domain adaptation in different ways, which achieved outstanding diagnosis results, proving the research on domain adaptive intelligence methods is effective and indispensable.

In the study of intelligent diagnosis algorithms, the existing methods show that considering the original data class structure of the data set can not only enhance the feature extraction ability of the model but also improve the reliability and stability of the model [18, 19]. Tao *et al* [20] proposed a novel bearing defect diagnosis model based on semi-supervised kernel local Fisher discriminant analysis, using the density peak clustering technique to generate pseudo-cluster labels to achieve the extraction of optimal classification features. Based on the method that preserved the local and global structures of the original data used by Yin and Yan [21], the final extracted features were the deep representation of the data. In addition, they preserved the structural information as much as possible. The model proposed by Zhao *et al* [22] paid more attention to the essential geometric features of the data and established a local constraint matrix and a non-local constraint matrix for the samples to mine the local and non-local multi-popular structure information of the data, which achieved favorable diagnostic results.

Inspired by the above ideas, much literature has also begun to consider the data class structure in domain adaptation to limit the transfer direction of the transfer model. Tian *et al* [23] proposed local feature learning based on the discriminative loss of the center. Although it can enhance the intra-class compactness and inter-class separability of the data, the proposed method was implemented based on mini-batch stochastic gradient descent, resulting in a demanding task. The inter-class repulsive force term was designed by Wang *et al* [24], whereas the strategy needs the assistance of target domain samples to obtain better results. Wang *et al* [16] used multi-scale advanced feature alignment to achieve intra-class transfer adaptation, but did not consider inter-class separation. Zou *et al* [25] constructed a novel inter-class and intra-class distance constraint for domain adaptation, but the core idea of this method is to randomly generate sample center matrices without considering original data features, such as the variance of the source domain. Based on the existing transfer fault diagnosis methods, the current domain adaptation focuses more on the difference in feature distribution of the source and target domains, which most likely ignores the data information features contained in the original data of the source domain. In this way, the performance of model feature reconstruction may be reduced. If the model has excellent feature reconstruction performance, the generated features deviate less from the original data, and the validity of the features increases. This being the case, in this paper, a nearest neighbor feature constraint (NNFC) strategy is proposed, which fully considers the feature information of the original data in the source domain as well as effectively enhances intra-class aggregation and out-of-class separation while minimizing the computational load. Combined with the nearest neighbor multiple-alignment strategy, it can achieve high precision and reliable fault diagnosis under different working conditions from the source domain without the target domain label. Based on the above, a transfer-learning fault diagnosis method is proposed considering NNFCs.

The contributions of the proposed method are summarized as follows:

(a) An NNFC strategy is proposed. The nearest neighbor samples are used to enhance the aggregation within the class and the separation outside the class. Meanwhile, the variance distance and sample distance are used to constrain the directionality of the network feature extraction, which can enhance the performance of feature extraction.
(b) A nearest neighbor multiple-alignment strategy is used for model distribution alignment to improve the degree of distribution alignment.
(c) A dynamic weight strategy is studied in this paper, improving the convergence of the loss function during the training process.
(d) Two sets of experiments are used to verify the performance of the method. Compared to other advanced methods, the proposed method has superior transfer performance, which can achieve reliable and stable fault diagnosis.

The rest of the paper is as follows: section 2 introduces the basic theory. Section 3 details the proposed intelligent fault diagnosis method. The performance verification of the proposed algorithm is presented in section 4. Finally, section 5 summarizes the research content of this paper.

2. Preliminary

2.1. Stacked autoencoder (SAE)

AE has been widely studied as a common unsupervised network [26]. Due to their unique structure, AEs can simply implement feature extraction from data. An AE is mainly composed of an encoder and a decoder, where the dimension of the data can be reduced by the encoder and the sample data can be reconstructed via the decoder. The reconstruction error E_{AE} of the AE is as follows:

$$E_{\mathrm{AE}} = \frac{1}{n}\sum_{i=1}^{n} \|x_i - \hat{x}_i\|^2, \tag{1}$$

where n is the number of samples, x_i is the ith group of sample data and $\widehat{x}_i$ is the ith group of reconstructed sample data.

However, a traditional AE has only a single hidden layer, which limits the feature extraction ability of AE in massive data. Therefore, an SAE is studied to improve the feature extraction performance of the traditional AE [27]. Although the SAE increases the number of hidden layers, its principle is still the same as that of the traditional AE. Thus, the reconstruction error E_{SAE} of SAE can be expressed as follows:

$$E_{\mathrm{SAE}} = \frac{1}{n}\sum_{i=1}^{n}\left\|x_i - \hat{x}_i\right\|^2 + \lambda\left\|w\right\|, \tag{2}$$

where λ is the weight factor and w is the network weight.

2.2. K nearest neighbors (KNNs)

KNN is a classic classification algorithm. Specifically, by calculating the KNNs of the samples in the data set, the method can judge the properties of the samples with the help of the properties of these neighborhoods [28]. The commonly used distance calculation formula is Euclidean distance, which is,

$$d = \sqrt{\sum_{i=1}^{m}(a(i) - b(i))^2}, \tag{3}$$

where a and b are two sets of samples, respectively, and m is the sample dimension.

It should be noted that the classification properties of KNN are not emphasized in this paper, whereas its nearest neighbor concept is mainly applied. In this paper, $\mathrm{KNN}(x,k)$ is used to denote the kth nearest neighbor of the sample x in the data set.

2.3. Maximum mean discrepancy (MMD)

As a common inter-domain distance metric, MMD has mature performance [29, 30], which measures the difference between the two domains by mapping the source domain and the target domain samples into the reproducing kernel Hilbert space (RKHS). If the metric value is small enough, the two domains can be considered to have the same distribution. After applying the feature kernel function $k(\cdot)$, the empirical estimate of the MMD metric can be expressed as follows:

$$\begin{aligned}\mathrm{MMD}(X^s, X^t) &= \left\|\frac{1}{n_s}\sum_{i=1}^{n_s}\mathbb{F}\left(d_i^s\right) - \frac{1}{n_t}\sum_{j=1}^{n_t}\mathbb{F}\left(d_j^t\right)\right\|_{\mathrm{RKHS}}^2 \\ &= \frac{1}{n_s n_s}\sum_{i=1}^{n_s}\sum_{j=1}^{n_s}k\left(d_i^s, d_j^s\right) + \frac{1}{n_t n_t}\sum_{i=1}^{n_t}\sum_{j=1}^{n_t}k\left(d_i^t, d_j^t\right) \\ &\quad - \frac{2}{n_s n_t}\sum_{i=1}^{n_s}\sum_{j=1}^{n_t}k\left(d_i^s, d_j^t\right).\end{aligned} \tag{4}$$

Among them, $\mathbb{F}$ is a class of mapping functions in RKHS, $D^s = \{d_i\}_{i=1}^{n_s}$ is the independent sample drawn from the source domain probability distribution X^s, $D^t = \{d_j\}_{j=1}^{n_t}$ is the independent sample drawn from the target domain probability distribution X^t, n_s is the number of samples in the source domain and n_t is the number of samples in the target domain. It should be clear that the feature kernel function applied in this paper is a Gaussian kernel function.

3. Proposed method

To enhance the feature extraction ability of the network and improve the applicability, a Transfer-Learning (NNFCTL) method considering the Nearest Neighbor Feature Constraints is proposed. The specific structure of the NNFCTL method is shown in figure 1.

3.1. NNFC strategy

Although the AE can simply reduce the dimensionality of the sample data, the direction of feature extraction is uncontrollable. Hence, to control the direction of model feature extraction, an NNFC strategy is proposed. The strategy is conceived from the perspective of nearest neighbor samples, in which the data features and structural features of the original data are estimated by the computed values of the nearest neighbor samples to enhance the effectiveness of the extracted features.

The schematic diagram of the data features of the sample is shown in figure 2(a), which consists of two parts: local features and global features. Local features mainly focus on features within a small range of samples. Specifically, for a group of sample points, the smaller the distance between the sample and its nearest neighbor, the tighter the sample distribution. The main goal of global features is to describe the overall characteristics of the data. Whereas variance is a typical data characteristic of a set of data, and to a certain extent can express the overall dispersion of a set of data. Thus, the variance is used to measure the difference between the samples before and after feature extraction, to ensure the similarity between the reconstructed feature set and the original sample set. As mentioned, the data feature E_{df} can be represented as follows:

$$E_{\mathrm{loc}} = \frac{1}{n_s}\sum_{i=1}^{n_s}\left\|d_i^s - \mathrm{KNN}(d_i^s, 1)\right\|^2 + \frac{1}{n_t}\sum_{j=1}^{n_t}\left\|d_j^t - \mathrm{KNN}(d_j^t, 1)\right\|^2, \tag{5}$$

$$\begin{aligned}E_{\mathrm{glo}} &= \left\|\sigma(D^s) - \sigma\left(\mathrm{KNN}(D^s, 1)\right)\right\|^2 \\ &\quad + \left\|\sigma(D^t) - \sigma\left(\mathrm{KNN}(D^t, 1)\right)\right\|^2,\end{aligned} \tag{6}$$

$$E_{\mathrm{df}} = E_{\mathrm{loc}} + E_{\mathrm{glo}}. \tag{7}$$

Among them, $D^s = \{d_i\}_{i=1}^{n_s}$ is the source domain samples, $D^t = \{d_j\}_{j=1}^{n_t}$ is the target domain samples n_s is the total number of source domain samples, n_t is the total number of target domain samples and $\sigma(\cdot)$ represents variance calculation. In this paper, $\mathrm{KNN}(x,k)$ is used to denote the kth nearest neighbor to the sample x in the data set.

In addition to the data features of the samples, the structural features of the samples are also considered, as shown in figure 2(b). After visualizing the samples in a 2D plane, the distances between the samples are visualized. For a classification model, increasing the distance between samples of different classes and decreasing the distance between samples

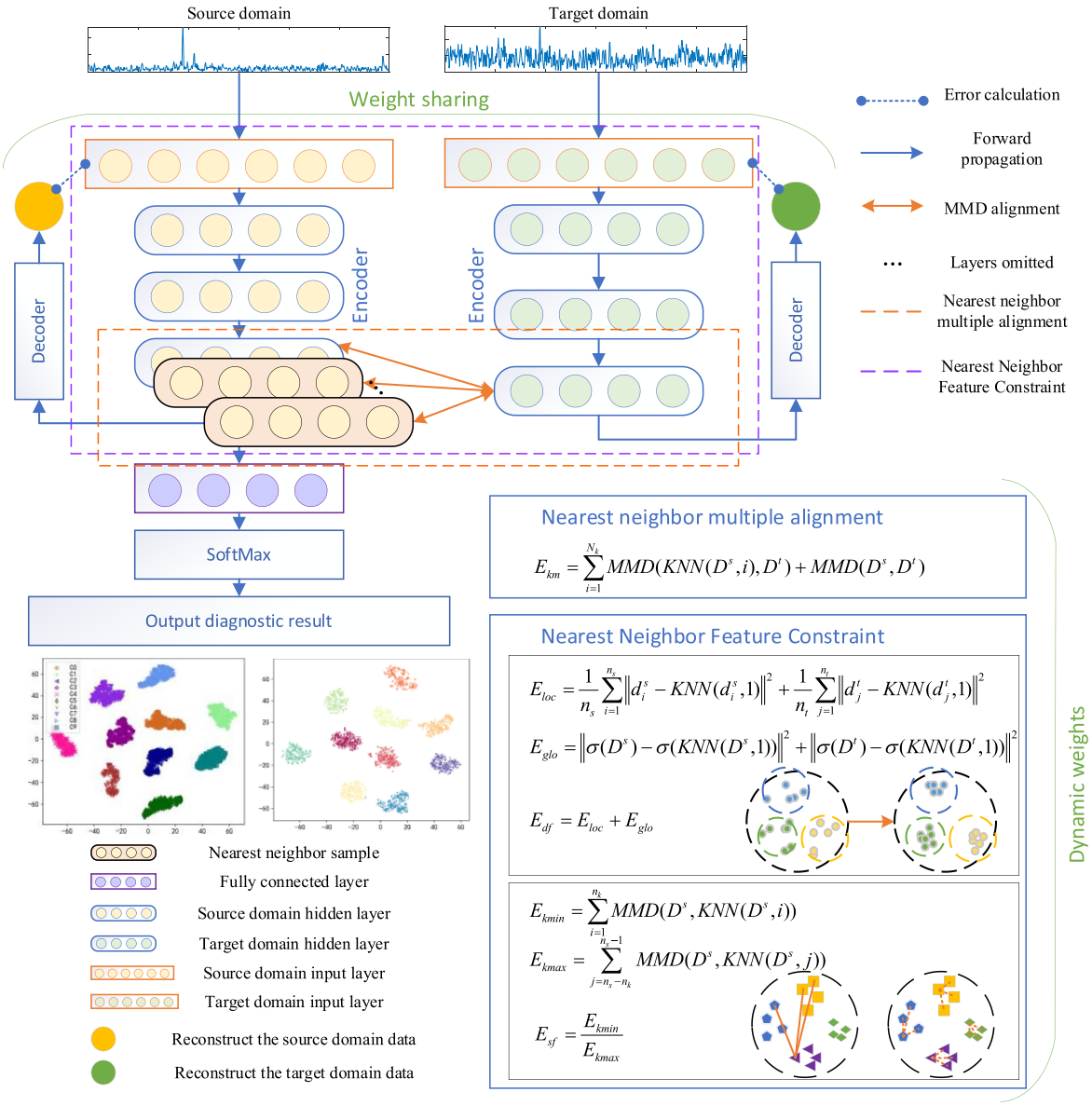

Figure 1. Detailed structure diagram of the proposed method: in this figure, a three-layer stacked AE is used as the basic structure of the model, in which the source and target domains share model weights. Then, after the third encoding layer, the fully connected and the softmax classification layers are connected to enhance the classification ability of the model. In addition, the nearest neighbor feature constraint is added at the third encoding layer. Meanwhile, the nearest neighbor multiple-alignment strategy is applied to the entire encoding layer of the model. Finally, a dynamic weight strategy is adopted for the above losses to improve efficiency.

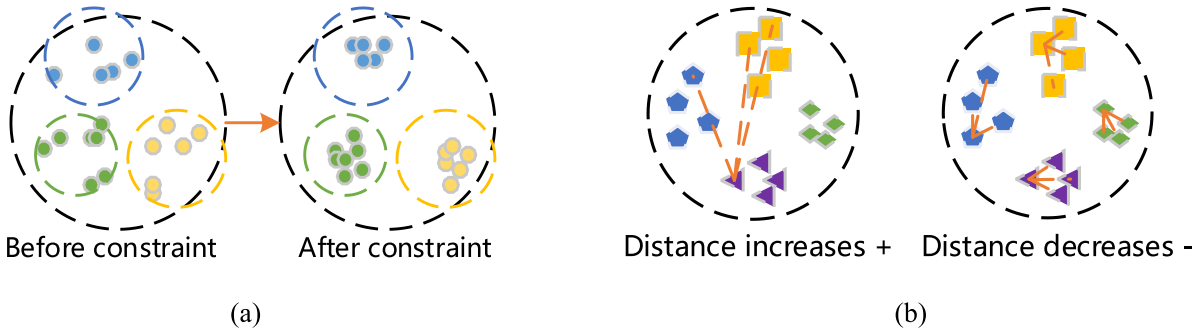

Figure 2. Schematic diagram of the nearest neighbor feature constraint strategy. (a) Schematic diagram of data feature constraint; (b) schematic diagram of structural feature constraint.

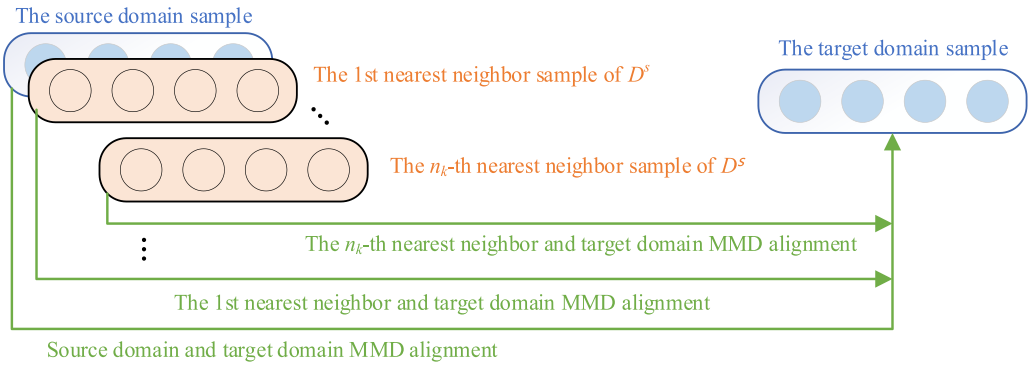

Figure 3. Schematic diagram of multiple-alignment strategy of nearest neighbor samples.

of the same class can enhance the model classification performance. Therefore, to achieve this goal, nearest neighbor samples are used to measure the inter-class and intra-class distances. By calculating the Euclidean distance between the sample and all other sample points in the set of data, the n_k group nearest neighbor sample with the closest distance to the sample and the n_k group nearest neighbor sample with the farthest distance is obtained. The intra-class aggregation is enhanced by reducing the distance between the sample and the nearest neighbor samples with close distances, and the out-class separation is enhanced by increasing the distance between the sample and the nearest neighbor samples with far distances, which constrains the feature reconstruction from the perspective of structure direction. Since the actual sample data are usually high-dimensional, MMD is chosen to measure the distance between the sample and the nearest neighbor sample. Hence, the structural feature E_{sf} is expressed by the following formula:

$$E_{k\min} = \sum_{i=1}^{n_k} \mathrm{MMD}\left(D^s, \mathrm{KNN}(D^s, i)\right), \tag{8}$$

$$E_{k\max} = \sum_{j=n_s-n_k}^{n_s-1} \mathrm{MMD}\left(D^s, \mathrm{KNN}(D^s, j)\right), \tag{9}$$

$$E_{\mathrm{sf}} = \frac{E_{k\min}}{E_{k\max}}, \tag{10}$$

where n_k represents the number of adjacent samples to be considered, which can be changed and set as needed. In this paper, this parameter is set to 3.

In general, NNFC is considered based on the characteristics of sample data and sample structure, which can constrain the direction of network feature reconstruction and enhance the reliability and effectiveness of features. The complete loss E_{NNFC} can be expressed as,

$$E_{\mathrm{NNFC}} = E_{\mathrm{df}} + E_{\mathrm{sf}}. \tag{11}$$

3.2. Multiple-alignment strategy of nearest neighbor samples

In practical applications, the probability distributions of the source and target domains are often different. Therefore, it is necessary to align the distributions of the source and target domains to achieve domain adaptation. To limit and reduce the difference between the distance between the source domain features and the target domain features, MMD is usually used to calculate them. However, only single correspondence alignment for single-layer samples may limit the degree of distribution alignment. Thus, a multiple-alignment strategy of nearest neighbor samples is used to improve the model, as shown in figure 3.

To enhance the adaptability of the network to the two domains, a strategy that calculates the nearest neighbor samples with the $1 \sim N_k$th closest distance to all samples in the source domain and aligns them with the target domain samples is used. The nearest neighbor sample multiple-alignment strategy can be expressed as,

$$E_{km} = \sum_{i=1}^{N_k} \mathrm{MMD}\left(\mathrm{KNN}(D^s, i), D^t\right) + \mathrm{MMD}(D^s, D^t), \tag{12}$$

where E_{km} is the multiple-alignment error of the nearest neighbor samples and N_k is the number of nearest neighbor alignments. It should be noted that the value of N_k is chosen to be 3, considering the computational cost and policy effect.

3.3. Dynamic weight strategy

At present, in the process of network training, the threshold of the total loss or the threshold of the number of iteration steps is usually used as the sign of the end of model training. When the total loss composition is simple, the above method shows reliable and stable performance. However, when the total loss consists of multiple constraints, although the total loss converges to a very low value, likely, one of the constraints has not reached a convergence state, which will affect the training effect of the model. To solve the above problems, a dynamic weight strategy is applied to this method to improve the convergence of the loss function. By assigning a dynamic weight value to the sub-constraint to change the proportion of the constraint in the total constraint items, it can be expressed by the following formula:

$$\mu = u(c, E) = c \cdot E. \tag{13}$$

Table 1. The model hyperparameter settings.

The NNFCTL default parameters					
Name	Iteration steps	Learning rate	Batch number of samples	Number of hidden layers	Activation function
Value	200	0.01	150	512-128-64	Sigmoid–Sigmoid–Sigmoid
Name	Weighting factor α	Weighting factor β	Weighting factor λ	Dynamic weight μ_1	Dynamic weight μ_2
Value	0.5	1	0.0004	$u\,(1, E_{km})$	$u\,(2.5, E_{\mathrm{NNFC}})$

Among them, c is a multiplication factor greater than 1, which can be set to different values for different sub-loss terms E and μ is the dynamic weight value, which changes dynamically with the sub-loss term E.

In a nutshell, the dynamic weight strategy makes the weights change as the value of the loss term changes. When the value of the sub-loss term is larger than the value of other sub-loss terms, the weight increases accordingly, and the convergence direction of the network model is inclined to increase the convergence of the loss function.

3.4. Transfer-learning method considering the nearest neighbor features

The proposed method applies the above strategy based on the traditional SAE, and the reconstruction error E_{TL} of the SAE with transfer learning is introduced as,

$$E_{\mathrm{TL}} = \frac{1}{n_s}\sum_{i=1}^{n_s}\left\|d_i^s - \widehat{d_i^s}\right\|^2 + \frac{1}{n_t}\sum_{j=1}^{n_t}\left\|d_j^t - \widehat{d_j^t}\right\|^2 + \lambda\|w\|, \quad (14)$$

where $\widehat{d_i^s}$ is the ith group of source domain reconstruction samples, $\widehat{d_j^t}$ is the jth group of target domain reconstruction samples, n_s is the total number of source domain samples and n_t is the total number of target domain samples.

However, traditional AE networks belong to typical unsupervised networks, which will affect the classification performance of the network. To enhance the classification ability of the network, label information is introduced to fine-tune the model, and the cross-entropy loss L_{sem} can be expressed as follows:

$$L_{\mathrm{sem}} = -\frac{1}{n_s}\sum_{i=1}^{n_s} y_i \times \log\hat{y}_i, \quad (15)$$

where y_i is the true label of the sample in the ith group and $\widehat{y}_i$ is the predicted label of the sample in the ith group.

Thus, the total loss E_{sum} of the proposed method is expressed as,

$$E_{\mathrm{sum}} = \alpha E_{\mathrm{TL}} + \beta L_{\mathrm{sem}} + \mu_1 E_{km} + \mu_2 E_{\mathrm{NNFC}}, \quad (16)$$

where α and β are weight factors, while μ_1 and μ_2 are the dynamic weights of loss E_{km} and loss E_{NNFC}, respectively. The hyperparameter settings of the model are shown in table 1. It should be noted that since E_{TL} contains the data of the source and the target domains, to balance the numerical value, E_{TL} should be halved. As a result, the weight factor α takes the value of 0.5. Because E_{TL} is an unsupervised term and L_{sem} is a supervised term, their weights are usually the same, and β is set to 1. Whereas the weight factor λ usually takes a very small value to avoid taking a large proportion of the loss function and affecting the model training. Regarding the dynamic weight factor, the setting method will be discussed in subsequent experiments.

3.5. Process of the proposed method

The specific steps of the transfer-learning method considering nearest neighbor features are shown in figure 4.

The main process is as follows:

(a) Vibration signal acquisition. Time-frequency conversion is performed on the data in the source and target domains, in which the training and the testing sets are divided.
(b) Construct an NNFCTL model and set the model hyperparameters.
(c) The labeled source domain training set and the unlabeled target domain training set are fed into the model for training.
(d) Calculate various loss functions, update the network weights iteratively, stop training when the threshold iteration steps are reached, and save the model.
(e) An unlabeled source domain testing set and an unlabeled target domain testing set are used to test the performance of the model.
(f) Output the extracted features and fault diagnosis results.

4. Experiment analysis

Two sets of experiments were conducted to investigate the performance of the transfer-learning method proposed in this paper considering nearest neighbor features.

4.1. Experiment 1

First, the rolling-bearing open data set from the Case Western Reserve University (CWRU) is selected to analyze the performance of the NNFCTL method. The experimental platform is shown in figure 5. In this experiment, the sampling frequency of the driving end is selected as 48 kHz experimental data, including four kinds of load conditions. For each load

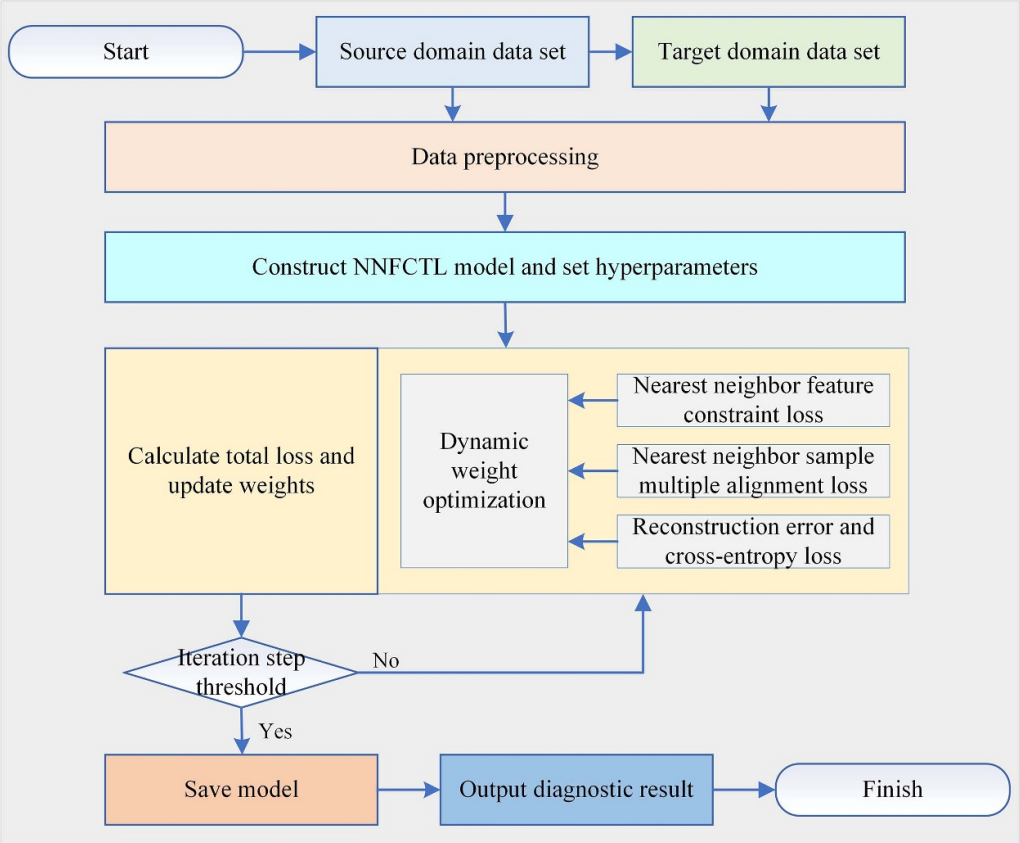

Figure 4. Overall flow chart of the proposed method.

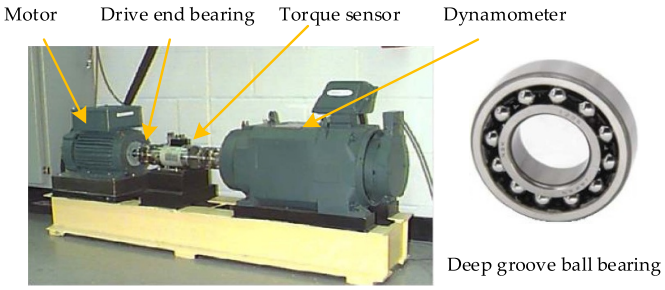

Figure 5. CWRU data set experiment platform.

condition, a total of ten fault degrees (including normal state) is selected, 600 groups of samples are selected for each fault degree, and the sample length of each group of samples is 600. The detailed data division table is shown in table 2. In addition, the ratio of the training set to the testing set in the data set is 1:1.

4.1.1. Validation of the NNFC strategy. To verify the effectiveness of the proposed NNFC strategy, a set of comparative experiments was designed, whose parameters were all consistent with those in table 1. Under the same data set and parameter settings, only the use of the NNFC strategy was changed, and the experimental results of the NNFCTL method and NNFCTL without the NNFC strategy were compared.

Table 2. The open data set detailed partition table.

Data set	Load (HP)	Type of failure	Depth of failure (mm)	Number of samples	Label
A/B/C/D	0/1/2/3	IF1	0.5334	600/600/600/600	0
		IF2	0.3556	600/600/600/600	1
		IF3	0.1778	600/600/600/600	2
		OF1	0.5334	600/600/600/600	3
		OF2	0.3556	600/600/600/600	4
		OF3	0.1778	600/600/600/600	5
		RF1	0.5334	600/600/600/600	6
		RF2	0.3556	600/600/600/600	7
		RF3	0.1778	600/600/600/600	8
		N	0	600/600/600/600	9

Since other strategies may affect the model and interfere with the experimental results, the weights of other strategies are set to 0 in this group of experiments. The t-distributed stochastic neighbor embedding (t-SNE) map can intuitively reflect the difference and similarity of features, so it is used to visualize features for comparison.

The experimental results of cases A–D and D–A are shown in figure 6. When comparing the two groups of transfer cases, the classification performance of the method with the NNFC strategy proved to be better than that without the NNFC strategy. The distances of different fault points in figures 6(a) and (c) are separated, and the boundaries are obvious. Most

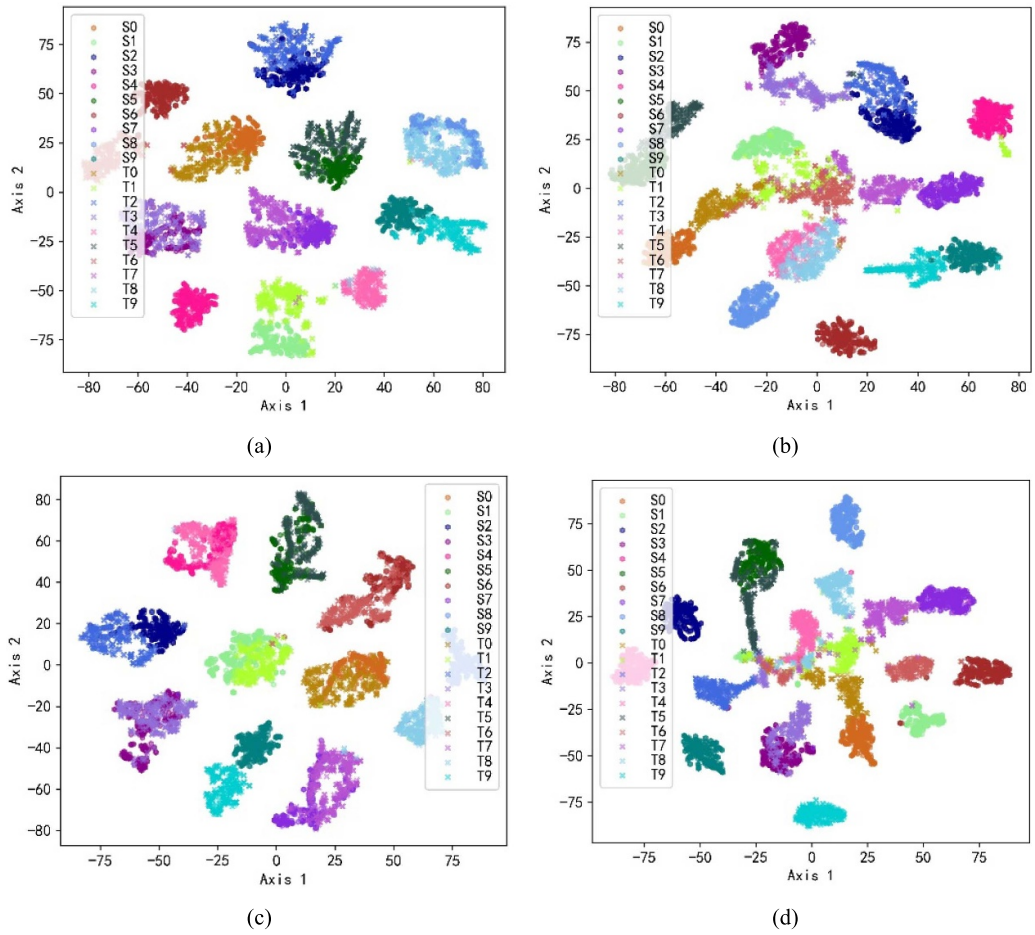

Figure 6. Performance analysis diagram of the nearest neighbor feature constraint strategy. (a) t-SNE diagram of NNFCTL in transfer case A–D; (b) t-SNE diagram of NNFCTL without NNFC strategy in transfer case A–D; (c) t-SNE diagram of NNFCTL in transfer case D–A; (d) t-SNE diagram of NNFCTL without NNFC strategy in transfer case D–A.

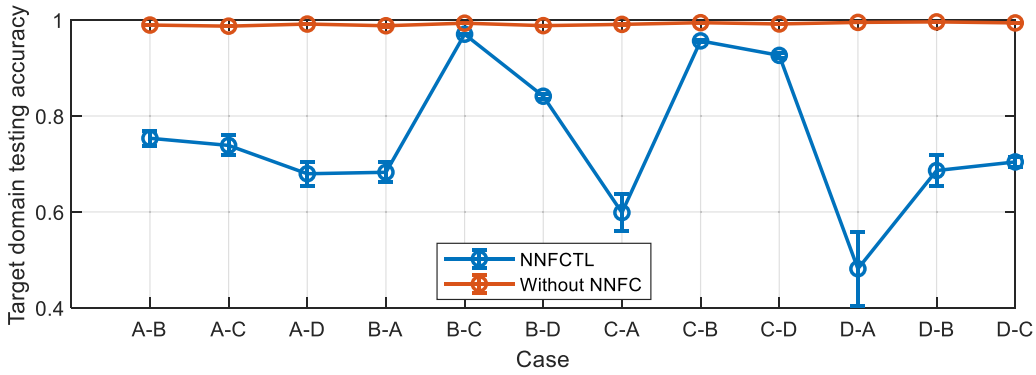

Figure 7. Error accuracy plot of the nearest neighbor feature constraint strategy in all transfer cases.

of the fault types of the source and target domains correspond one-to-one, and if they do not correspond, they can also be separated from other fault types. While figures 6(b) and (d) show experimental results without the NNFC strategy, many fault points are mixed, the classification boundaries are not clear, and the original data features are lost. From the comparison results, it can be seen that the NNFC strategy can enhance the effectiveness of features and increase the difference between different types of data, which also has a positive impact on the transfer performance of the model. Overall, the NNFC strategy can improve the feature extraction ability of the model.

The accuracy error plots of the method with and without the NNFC strategy in all cases are shown in figure 7. In addition to depicting the mean of the ten-run precision, the fluctuation range of the ten-run precision is depicted. The NNFC strategy improves the diagnostic accuracy of the model in all transfer

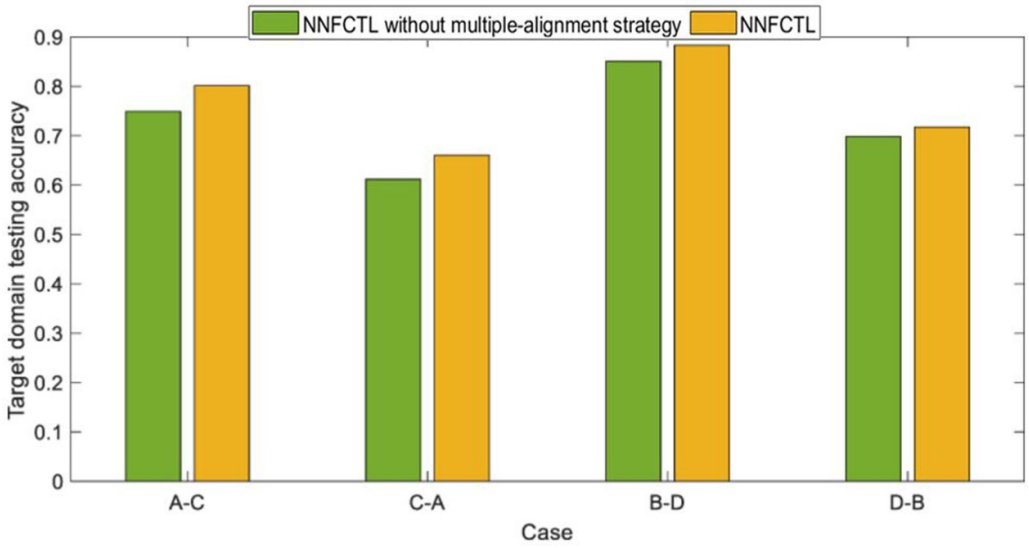

Figure 8. Impact of multiple-alignment strategy of nearest neighbor samples on the test accuracy of the target domain.

cases, whereas it improves the diagnostic stability, providing an obvious positive effect on the model.

4.1.2. Verification of multiple-alignment strategy for nearest neighbor samples. We continue to analyze the impact of the nearest neighbor sample multiple-alignment strategy on the model. Using all the same parameters, the NNFCTL method is compared to the NNFCTL method without the multiple-alignment strategy. Considering that other strategies will have a positive effect on the model while using the parameters in table 1, the weights of other strategies are set to 0. The experimental results are shown in figure 8.

Four groups of transfer cases are randomly selected, and the results in this figure show that the multiple-alignment strategy of nearest neighbor samples can achieve higher transfer accuracy under the same number of iteration steps. Although the accuracy improvement of the method applying the multiple-alignment strategy is not as pronounced as other strategies, it still has a positive effect on the model.

4.1.3. Dynamic weight strategy verification. The influence of dynamic weight strategies is analyzed with the help of the convergence value of the loss function. Under the same parameter settings, only the usability of the dynamic weight strategy is changed, and the results of the loss function are analyzed. The comparison results for all cases are shown in figure 9. The results show that the dynamic weight strategy can reduce the convergence value of the loss function and increase the convergence of the loss function during training. Specifically, the red line is overall higher than the blue line, indicating that the loss function without dynamic weight strategy does not converge to the lowest value during training. In terms of volatility, the red line has a large fluctuation range and is unstable and cannot guarantee the convergence of training, while the blue line has relatively small fluctuations, is smooth. In addition, the overall value is lower than

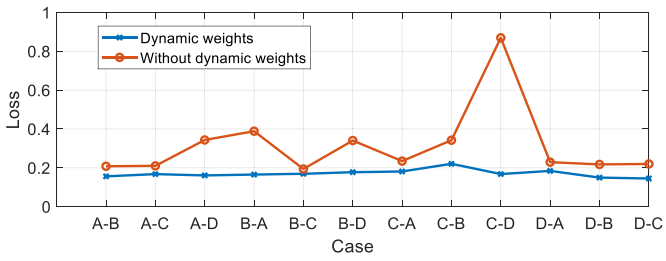

Figure 9. Impact of the dynamic weight strategy on the loss function of all cases.

the red line, indicating that the dynamic weight strategy can slow down the randomness of the loss function convergence degree and increase the degree of convergence. In summary, after adopting the dynamic weight strategy, the convergence of the loss function during the training process can be significantly enhanced, and the convergence stability of multiple sets of cases can be ensured at the same time.

4.1.4. Comparison of different methods. To further illustrate the performance of the proposed method, some advanced related research methods are used for comparative experiments, namely ATAE [31], CAETL [32], DTL [33] and SAECSDF [34]. It is worth noting that the parameter settings of these methods all adopt the optimal parameters stated in the literature, while the parameters of the proposed method adopt the default parameters in table 1. Considering that the accuracy of a single experiment is accidental, the average results of ten consecutive experiments are used for comparison in this experiment, and the specific accuracy is shown in table 3.

From the data in the table, in all cases, NNFCTL achieved the best average accuracy of transfer diagnosis, and the lowest average accuracy of 95.70%, showing the overall accuracy, stability and generalization. The best-performing method among the comparison methods is ATAE, with an average accuracy higher than 91% in all cases, but the proposed

Table 3. The experimental results of different methods in CWRU data sets.

Source domain	Method	Target domain			
		A	B	C	D
A	ATAE	—	91.23% ± 5.57%	92.99% ± 2.87%	94.62% ± 2.48%
	CAETL	—	59.84% ± 5.63%	55.09% ± 6.24%	52.17% ± 12.83%
	DTL	—	76.47% ± 5.09%	72.65% ± 6.38%	45.67% ± 32.90%
	SAECSDF	—	79.58% ± 5.62%	79.77% ± 3.73%	77.39% ± 2.05%
	NNFCTL	**—**	**97.04% ± 1.46%**	**96.19% ± 1.41%**	**97.31% ± 0.73%**
B	ATAE	94.73% ± 2.37%	—	91.92% ± 4.71%	95.93% ± 1.40%
	CAETL	68.77% ± 7.13%	—	78.81% ± 5.32%	64.22% ± 3.78%
	DTL	77.95% ± 8.92%	—	89.56% ± 6.00%	64.27% ± 27.50%
	SAECSDF	72.55% ± 3.48%	—	97.14% ± 1.33%	92.01% ± 2.29%
	NNFCTL	**95.70% ± 2.56%**	**—**	**98.11% ± 0.83%**	**97.24% ± 0.80%**
C	ATAE	96.04% ± 1.72%	93.91% ± 1.89%	—	96.50% ± 1.57%
	CAETL	66.10% ± 1.60%	75.23% ± 10.40%	—	65.15% ± 4.45%
	DTL	72.98% ± 7.42%	82.50% ± 15.03%	—	78.92% ± 14.91%
	SAECSDF	74.22% ± 4.85%	97.41% ± 0.96%	—	94.62% ± 1.38%
	NNFCTL	**96.30% ± 2.17%**	**98.96% ± 0.67%**	**—**	**97.08% ± 1.62%**
D	ATAE	94.50% ± 3.57%	91.34% ± 4.26%	94.34% ± 2.22%	—
	CAETL	63.06% ± 8.51%	71.57% ± 7.16%	71.67% ± 5.77%	—
	DTL	35.60% ± 44.47%	63.38% ± 28.85%	70.41% ± 22.39%	—
	SAECSDF	79.52% ± 5.01%	88.98% ± 5.79%	93.49% ± 2.07%	—
	NNFCTL	**98.82% ± 0.75%**	**98.47% ± 1.06%**	**98.79% ± 0.51%**	**—**

Note: In order to improve the readability, the experimental results of the proposed method are bold.

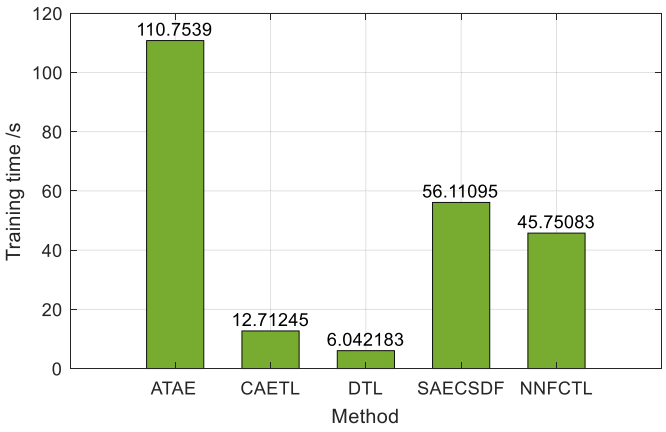

Figure 10. Computation time of different methods in transfer case A–D.

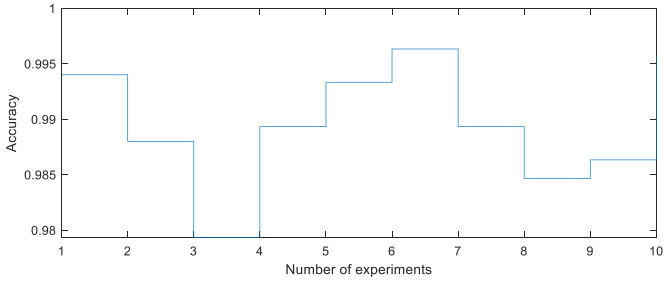

Figure 11. Results of ten consecutive experiments of the NNFCTL method in case C–B.

method still shows better accuracy compared to it. Moreover, the comparison methods show a large difference in the accuracy of the same case in most cases, and the NNFCTL method only has a slightly larger accuracy difference than the same case in individual cases. In conclusion, the proposed method still shows certain stability. Although all comparison methods can achieve high accuracy in some cases, compared to all cases, the proposed method can achieve high accuracy in all cases, which reflects the generalization of the NNFCTL method. Specifically, when data set A is used as the target domain, the transfer performance of most of the methods is degraded, but the proposed method can still achieve satisfactory results, indicating that it has a certain anti-interference in the transfer process.

The training time results for different methods are shown in figure 10. CAETL and DTL are the least time-consuming models because they use the transfer achieved by the parameter fine-tuning method. Although they gain high computational efficiency, there is a slight loss in migration diagnostic performance for complex operating conditions. While ATAE consumes the longest amount of time, the use of KNN supervised classification improves the diagnostic accuracy but also increases the computational cost. In addition, the SAECSDF method also considers the in-class and out-of-class structures, so the model computation consumption increases compared to the parameter fine-tuning class. Compared to the SAECSDF method, the proposed method shortens the calculation time, indicating that it can minimize the time consumption while considering the enhancement of the feature extraction performance of the model. Therefore, compared to the parameter fine-tuning class model, the NNFCTL method sacrifices part of the computation time to improve the reliability and stability of the model in complex transfer cases.

In addition to focusing on the overall performance of the proposed method in all transfer cases, the performance of a set of cases is also of concern. Figure 11 is a graph of the ten

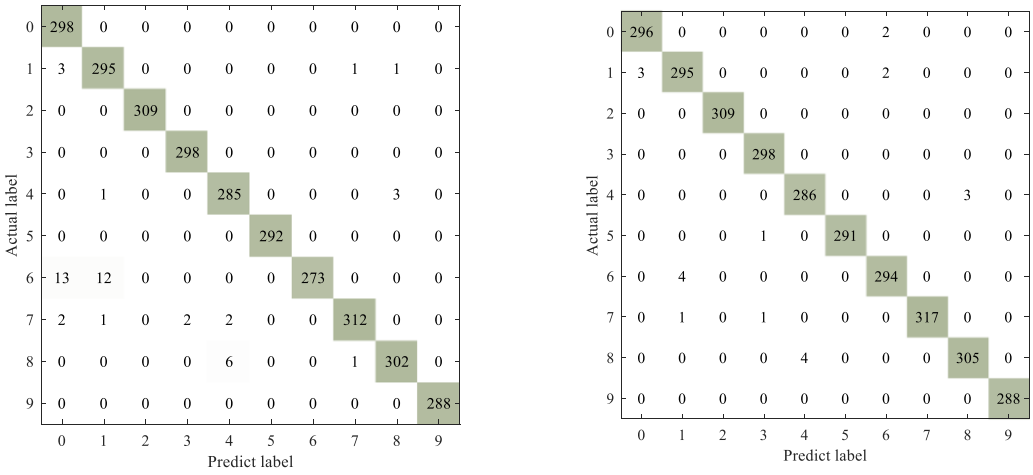

(a) (b)

Figure 12. Confusion matrix of the proposed method in the target domain of some transfer cases. (a) Confusion matrix diagram in transfer case B–D; (b) confusion matrix diagram in transfer case D–B.

consecutive transfer results of the proposed method in case C–B. From the data point of view, the maximum difference between the upper and lower fluctuations of the transfer accuracy is 0.017, and the difference between multiple experiments is very small. From the graphical point of view, the waveform is relatively flat, and there is no obvious strong peak. Consequently, results show that the NNFCTL method also has reliability and stability in the same transfer case.

The confusion matrix is often used to analyze the fault diagnosis performance of the diagnostic method. The confusion matrix of the proposed method in case B–D and case D–B is shown in figure 12. In figure 12(a), categories 0, 2, 3, 5 and 9 all achieved 100% transfer accuracy, among which category 6 has the largest transfer error, with an intra-class error accuracy of 8.38%, and other categories only have individual transfer errors. In summary, 98.4% accuracy was achieved in case B–D. However, in figure 12(b) the misclassification rate for all categories is very low, no large transfer error occurs, and the overall transfer accuracy is 99.3%. The evidence indicates that the proposed method has excellent transfer performance.

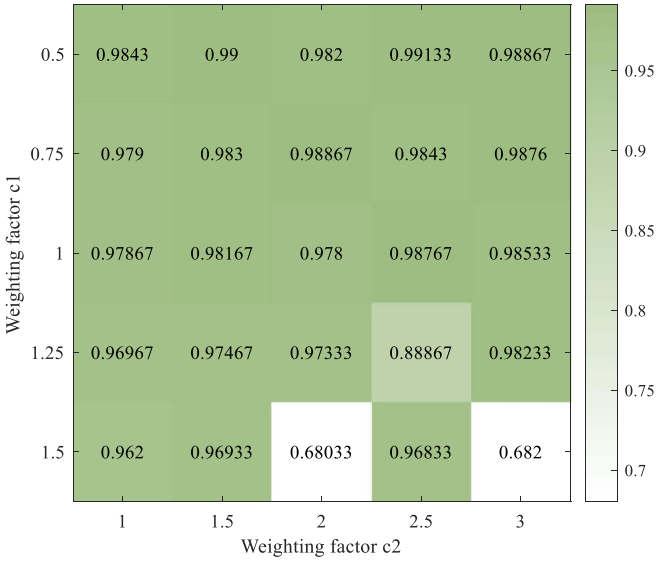

Figure 13. Results of different parameters in the target domain of transfer case A–D.

4.1.5. Weight factor selection. The optimal weights of the proposed method are described in table 1, and this section mainly discusses the selection of dynamic weights μ_1 and μ_2. It can be seen from the previous description that the dynamic weight μ is determined by the fixed factor c and the loss function value E. To increase the decisive role of E, it is appropriate to choose a value greater than 1 for c. To explore the best values of c_1 and c_2, several sets of experiments were carried out in the transfer case A–D, and the experimental results are shown in figure 13. Among them, the value ranges of c_1 and c_2 were in $[0.5, 1.5]$ and $[1, 3]$, respectively. Although higher accuracy can be obtained when c_1 is set to 0.5, considering the comprehensive dynamic weight strategy, $c_1 = 1$ and $c_2 = 2.5$ are selected as the optimal parameters.

4.2. Experiment 2

In addition to validation with the CWRU data set, a private data set is also used to analyze the performance of the proposed method. The experimental platform and bearing failure graph are shown in figure 14. For the private data set, data with rotational speeds of 900, 1000, 1200 and 1500 r min^{-1} were selected for experiments, respectively. Different rotational speed differences between transfer cases can better test the performance of the diagnostic method. In the above data

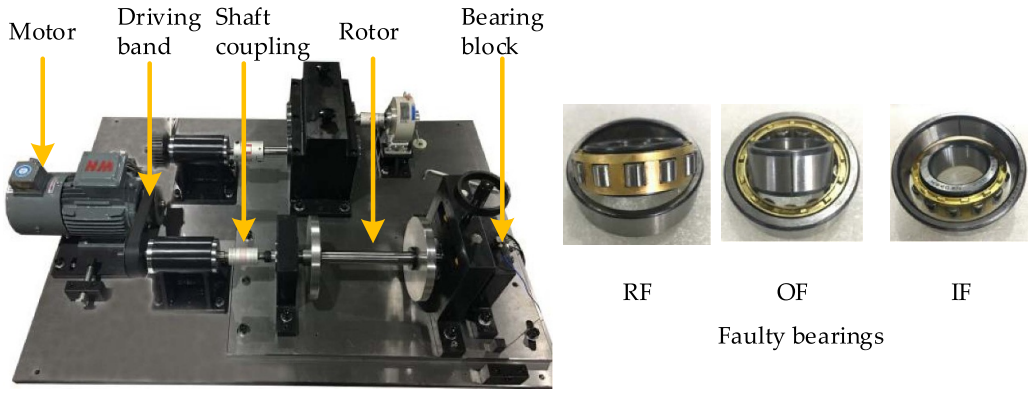

Figure 14. Private data set experiment platform.

Table 4. The private data set detailed partition table.

Data set	Load (rpm)	Type of failure	Depth of failure (mm)	Number of samples	Label
E/F/G/H	900/1000/1200/1500	IF	0.500	1500/1500/1500/1500	0
		OF	0.500	1500/1500/1500/1500	1
		RF	0.500	1500/1500/1500/1500	2
		N	0	1500/1500/1500/1500	3

set, a total of four fault types (including normal state) is selected, the number of samples for each fault type is 1500, and the length of each group of samples is 600. The specific data division table is shown in table 4. Likewise, the ratio of the training set to the testing set is still 1:1.

4.2.1. Validation of the NNFC strategy. Similar to the previous set of experiments, the method without the NNFC strategy is compared to the proposed method to verify the ability of the NNFC strategy. The parameter settings were the same as in the previous section. The t-SNE diagrams for transfer case E–H and transfer case H–E are shown in figure 15, and the results show that the NNFC strategy can make the feature difference more obvious. Clearly, in figures 15(a) and (c), different types of fault points can be well separated, most of the points with the same fault can be aggregated, and most of the data points of the source and the target domains can overlap in nearby places. While in figures 15(b) and (d) without NNFC strategy, although most of the data points can be separated, a few data points with different faults are crossed or misclassified. The correspondence between the sample points in the source and the target domains is relatively poor; most of them are just closer together with less overlap. To summarize, the NNFC strategy has a restrictive effect on model feature reconstruction and can effectively improve data intra-class aggregation and inter-class separation.

The effectiveness of the NNFC strategy is also verified in all the transfer cases in the private data set, and the results are shown in figure 16. In most cases, the NNFC strategy can improve fault diagnosis accuracy. In particular, the model with the NNFC strategy has small fluctuations in accuracy in ten consecutive experiments, and the diagnostic results are stable, proving that the NNFC strategy has superior performance.

4.2.2. Verification of multiple-alignment strategy for nearest neighbor samples. To further verify the impact of the multiple-alignment strategy for nearest neighbor samples, a validation test is also performed on the private data set. In the same way, the parameters in table 1 were applied to the basic parameters, and the weights of other strategies were reduced to 0 to avoid the interference of other strategies in the experiment. The experimental results for four groups of randomly selected transfer cases are shown in figure 17. In this picture, there is always a height difference between the green and yellow columns, which indicates that the multiple-alignment strategy of the nearest neighbor samples has a positive influence on the accuracy of the model transfer, improving the model transfer ability to a certain extent.

4.2.3. Dynamic weight strategy verification. Similarly, the performance of the dynamic weight strategy is verified and analyzed through controlled experiments. The converged value of the loss function is still used for further analysis, and the results for the transfer case in the private data set are shown in figure 18. From a local point of view, the case loss value of the low-speed data sets E and F as the source domain is larger, and the role of the dynamic weight strategy is reflected at this time. Meanwhile, the high-speed

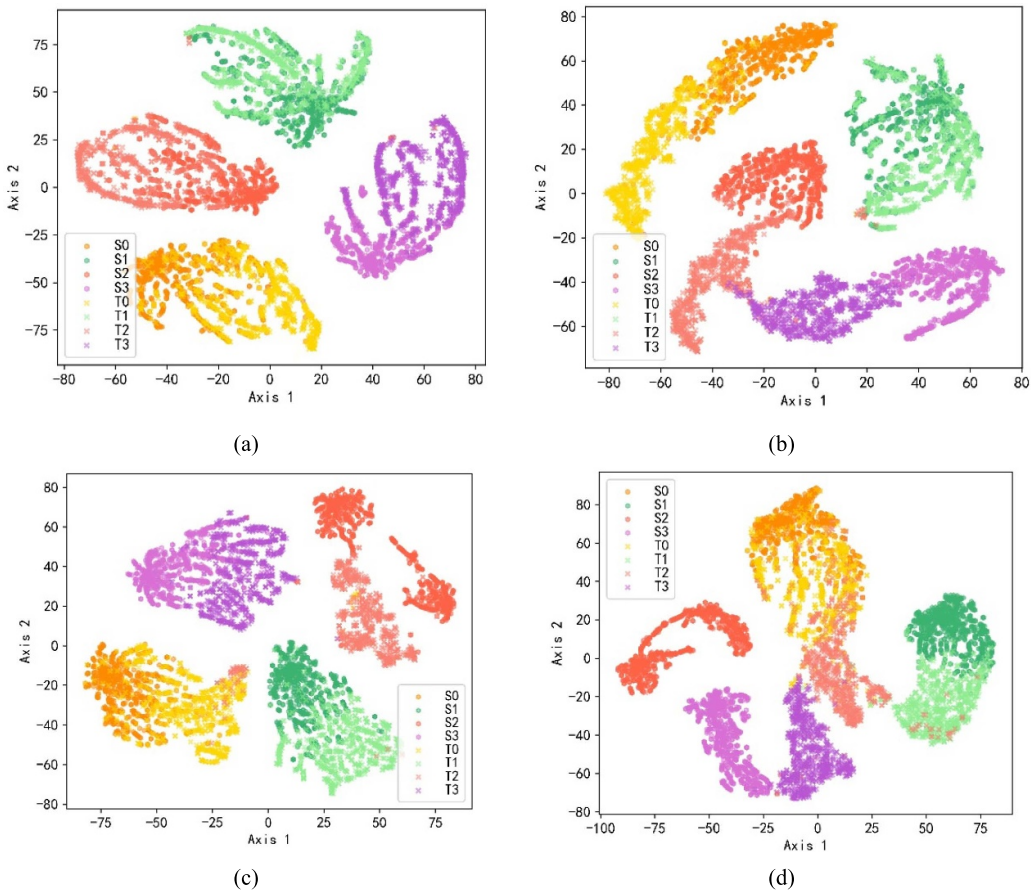

Figure 15. Performance analysis diagram of the nearest neighbor feature constraint strategy. (a) t-SNE diagram of NNFCTL method in transfer case E–H; (b) t-SNE diagram of NNFCTL method without NNFC strategy in transfer case E–H; (c) t-SNE diagram of NNFCTL method in transfer case H–E; (d) t-SNE diagram of NNFCTL method without NNFC strategy in transfer case H–E.

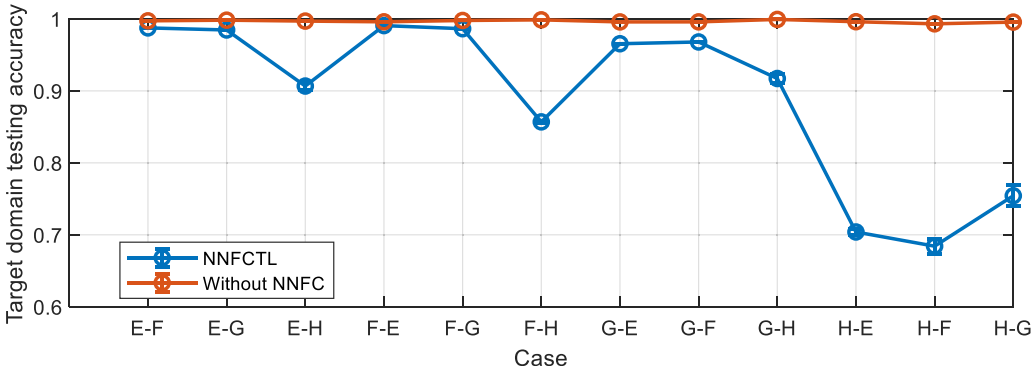

Figure 16. Error accuracy plot of the nearest neighbor feature constraint strategy in all transfer cases.

data sets G and H are used as the source domain, and the red line also shows minor differences to the blue line. Overall, the blue line is lower than the red line, and the line is smooth, still showing stability. Therefore, the comparison results show that the dynamic weight strategy reduces the convergence value of the loss function while ensuring that the convergence value of the model does not differ too much in all cases, increasing the convergence stability of the model.

4.2.4. Comparison of different methods. Furthermore, other advanced research methods are selected for performance comparison, and the comparison method is the same as the previous set of experiments. It should be noted that the parameter settings of all methods are also the same as in the previous set of experiments. To avoid contingency in the experiments, the average results of ten consecutive experiments were selected for the experimental results, and the experimental results of different methods are shown in table 5.

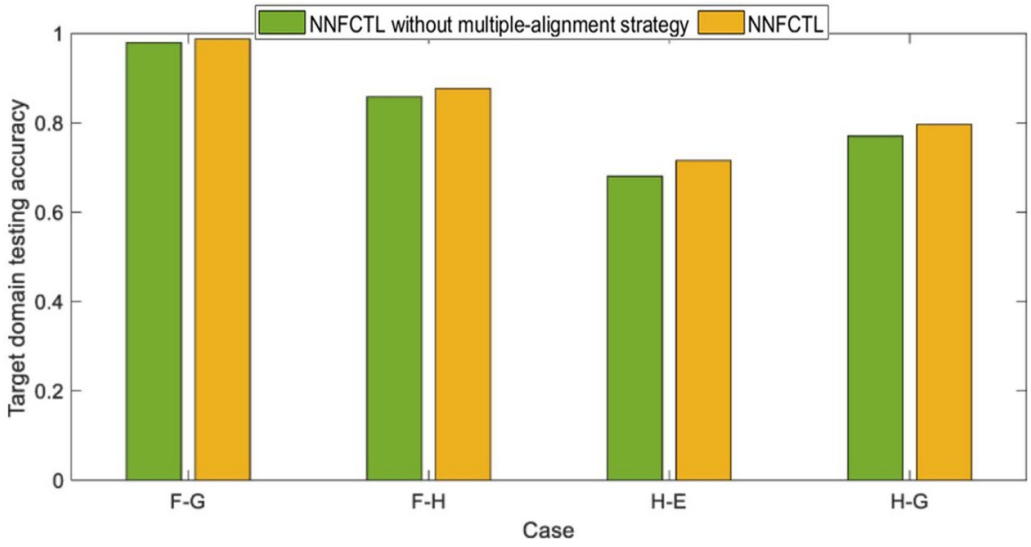

Figure 17. Impact of multiple-alignment strategy of nearest neighbor samples on the test accuracy of the target domain.

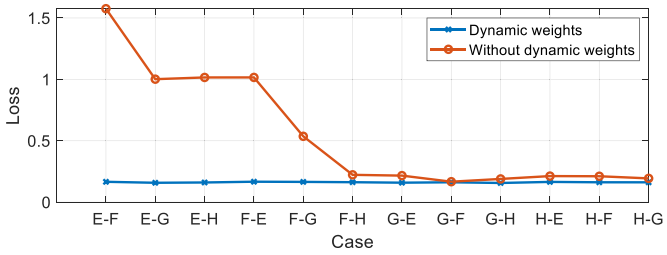

Figure 18. Impact of the dynamic weight strategy on the loss function of all cases.

Table 5. The experimental results of different methods in private data sets.

Source domain	Method	Target domain			
		E	F	G	H
E	ATAE	—	78.52% ± 14.82%	79.04% ± 12.66%	89.13% ± 5.37%
	CAETL	—	98.46% ± 0.50%	97.56% ± 1.30%	96.63% ± 2.17%
	DTL	—	91.57% ± 8.00%	98.30% ± 1.33%	93.91% ± 5.59%
	SAECSDF	—	98.98% ± 0.56%	98.58% ± 0.56%	94.99% ± 3.17%
	NNFCTL	**—**	**99.71% ± 0.09%**	**99.69% ± 0.21%**	**99.75% ± 0.12%**
F	ATAE	77.46% ± 13.04%	—	83.94% ± 8.99%	88.48% ± 9.05%
	CAETL	98.42% ± 0.61%	—	98.63% ± 0.50%	98.62% ± 0.48%
	DTL	95.79% ± 3.15%	—	98.78% ± 0.79%	93.68% ± 5.69%
	SAECSDF	98.21% ± 0.73%	—	98.45% ± 0.62%	92.93% ± 3.70%
	NNFCTL	**99.44% ± 0.16%**	**—**	**99.64% ± 0.13%**	**99.81% ± 0.13%**
G	ATAE	76.57% ± 12.43%	77.36% ± 12.70%	—	90.19% ± 6.14%
	CAETL	96.67% ± 1.23%	95.88% ± 1.75%	—	99.10% ± 0.54%
	DTL	97.59% ± 1.28%	96.32% ± 2.45%	—	97.68% ± 2.19%
	SAECSDF	97.31% ± 0.89%	97.32% ± 0.61%	—	95.67% ± 2.93%
	NNFCTL	**99.27% ± 0.33%**	**99.11% ± 0.22%**	**—**	**99.77% ± 0.13%**
H	ATAE	73.92% ± 15.58%	71.39% ± 6.55%	83.66% ± 11.30%	—
	CAETL	88.52% ± 3.81%	89.83% ± 4.47%	91.93% ± 3.14%	—
	DTL	91.84% ± 5.60%	86.37% ± 9.73%	95.29% ± 3.81%	—
	SAECSDF	90.42% ± 4.68%	93.50% ± 3.00%	95.86% ± 1.37%	—
	NNFCTL	**98.46% ± 0.71%**	**98.78% ± 0.29%**	**99.20% ± 0.27%**	**—**

Note: In order to improve the readability, the experimental results of the proposed method are bold.

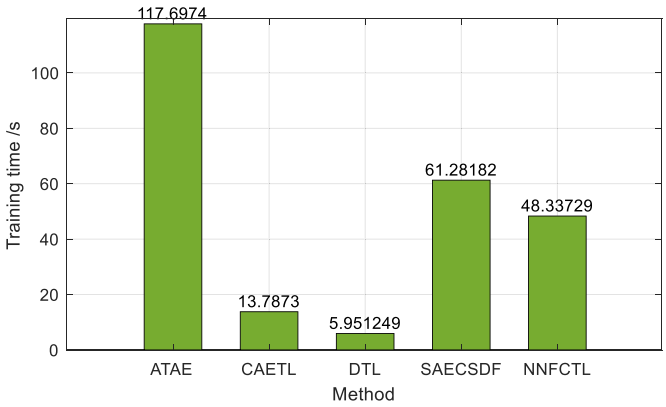

Figure 19. Computation time of different methods in transfer case E–H.

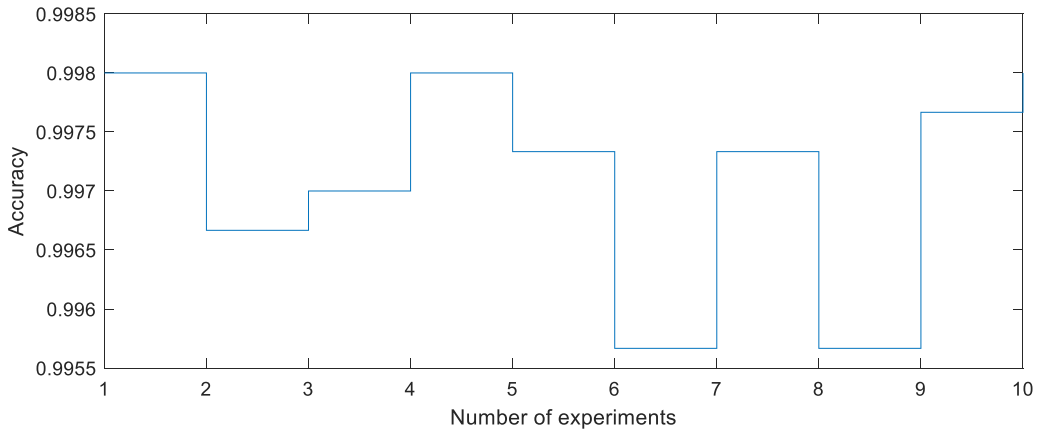

Figure 20. Results of ten consecutive experiments of the NNFCTL method in case E–F.

From the data analysis in the table, despite other methods showing high transfer accuracy in most cases, the proposed method still achieved the best diagnostic results in each transfer case, indicating reliability and generalization of the method. The rotational speed difference is different between different cases, and the data set H as the source domain brings the greatest challenge to the transfer. Compared to other data sets as the source domain, all methods have a certain degree of reduction in the transfer accuracy in the source domain H, while the NNFCTL method has the smallest reduction in accuracy, showing a certain degree of anti-interference. It is worth noting that the ATAE method performed the best among the comparison methods in the previous set of experiments, while other comparison methods performed better in this group of experiments, which shows that the comparison methods have different transfer performances for different data sets. Thus, the NNFCTL method shows stable performance in both sets of experiments, reflecting the generalization of the method.

The training time of all methods in the private data set is shown in figure 19. It can be seen from the data that most of the methods consume a longer amount of time than the CWRU data set, but the overall trend has not changed, indicating that the experimental results can illustrate the computational efficiency of the above methods. From the experimental results, the proposed method enhances the reliability and stability of the model while minimizing redundant computational consumption.

To verify the stability of the proposed method in the same case, the experimental results plotted in case E–F for ten consecutive times are shown in figure 20. Similarly, from the data analysis, the maximum difference is 0.0024, and the difference in the transfer accuracy is very small. From the graphical analysis, there is no obvious abrupt peak, and it is relatively smooth. The above evidence shows that the method has stability and reliability in the same set of the transfer cases.

In addition, the confusion matrix diagram of cases F–H and H–F is drawn to analyze the diagnostic performance, as shown in figure 21. In figure 21(a), there are only four misclassified samples in category 2, and the rest all achieve 100% transfer accuracy. Meanwhile, in figure 21(b), although the misclassification rate of category 2 is relatively large, which is 1.73%, the overall transfer accuracy rate reaches 99.14%. Thus, the confusion matrix results show that NNFCTL has high accuracy and enables reliable transfer diagnosis.

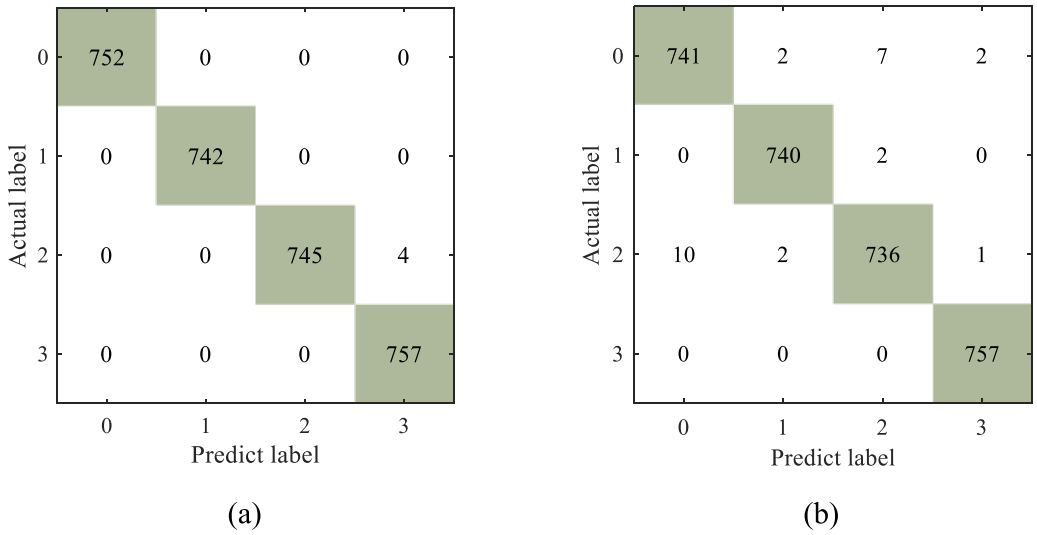

Figure 21. Confusion matrix of the proposed method in the target domain of some transfer cases. (a) Confusion matrix diagram in transfer case F–H; (b) confusion matrix diagram in transfer case H–F.

5. Conclusion

A transfer-learning fault diagnosis method considering NNFCs is proposed, which can constrain the direction of feature reconstruction, improve the adaptive ability of the model domain, and achieve reliable and accurate fault diagnosis. The method is also verified using two sets of experimental platform data, and the specific conclusions are as follows:

(a) The proposed NNFC strategy can effectively constrain the direction of network feature reconstruction and enhance feature effectiveness and feature extraction capabilities.
(b) The proposed multiple-alignment strategy of nearest neighbor samples can optimize the domain adaptation performance of the network.
(c) The dynamic weight strategy can effectively optimize the convergence of the loss function and enhance the stability of the model.
(d) Compared to different methods, the proposed method in this paper shows reliable transfer performance in both sets of experimental cases, which achieves stable diagnostic accuracy, with results indicating that the NNFCTL method has reliability, stability and generalization in fault diagnosis.

Although the proposed method can improve the performance of model feature extraction, it increases the computational consumption to a certain extent. Hence, how to balance the computational cost and the stability of diagnostic accuracy is an issue that needs further consideration. In addition, the selection of parameters also depends on experience, and how to obtain optimal parameters intelligently is also a problem that needs to be considered. In the future, further research will be conducted on the above issues.

Data availability statement

The data generated and/or analyzed during the current study are not publicly available for legal/ethical reasons but are available from the corresponding author on reasonable request.

Acknowledgments

We gratefully acknowledge all the participants, who assisted the successful completion of this study. It was funded by the Postgraduate Research and Practice Innovation Program of Jiangsu Province (Grant No. KYCX21_0230), the National Natural Science Foundation of China (Grant No. 51975276), the Special Project of National Key Research and Development Program of China (Grant No. 2020YFB1709801) and the Stability Support Project of Sichuan Gas Turbine Research Institute of AECC (Grant No. WDZC-2020-4-7).

ORCID iDs

Mengjie Zeng https://orcid.org/0000-0002-7815-9586
Kun Xu https://orcid.org/0000-0001-7827-2637

References

[1] Xu K, Li S, Li R, Lu J and Zeng M 2021 Deep domain adversarial method with central moment discrepancy for intelligent transfer fault diagnosis *Meas. Sci. Technol.* **32** 124005
[2] Li R, Li S, Xu K, Li X, Lu J, Zeng M, Li M and Du J 2022 Adversarial domain adaptation of asymmetric mapping with CORAL alignment for intelligent fault diagnosis *Meas. Sci. Technol.* **33** 055101
[3] Yang J, Bao W, Li X and Liu Y 2022 Improved graph-regularized deep belief network with sparse features

learning for fault diagnosis *Neural Comput. Appl.* **34** 9885–99
[4] Wang H, Xu J, Sun C, Yan R and Chen X 2022 Intelligent fault diagnosis for planetary gearbox using time-frequency representation and deep reinforcement learning *IEEE/ASME Trans. Mechatronics* **27** 985–98
[5] Hu Z, Han T, Bian J, Wang Z, Cheng L, Zhang W and Kong X 2022 A deep feature extraction approach for bearing fault diagnosis based on multi-scale convolutional autoencoder and generative adversarial networks *Meas. Sci. Technol.* **33** 065013
[6] Luo X, Li X, Wang Z and Liang J 2019 Discriminant autoencoder for feature extraction in fault diagnosis *Chemometr. Intell. Lab. Syst.* **192** 103814
[7] Cui M, Wang Y, Lin X and Zhong M 2021 Fault diagnosis of rolling bearings based on an improved stack autoencoder and support vector machine *IEEE Sens. J.* **21** 4927–37
[8] Wu X, Zhang Y, Cheng C and Peng Z 2021 A hybrid classification autoencoder for semi-supervised fault diagnosis in rotating machinery *Mech. Syst. Signal Process.* **149** 107327
[9] Long J, Chen Y, Yang Z, Huang Y and Li C 2022 A novel self-training semi-supervised deep learning approach for machinery fault diagnosis *Int. J. Prod. Res.* **60** 1–14
[10] Nguyen V, Cheng J and Thai V 2022 Stacked auto-encoder based feature transfer learning and optimized LSSVM-PSO classifier in bearing fault diagnosis *Meas. Sci. Rev.* **22** 177–86
[11] Haidong S, Ziyang D, Junsheng C and Hongkai J 2020 Intelligent fault diagnosis among different rotating machines using novel stacked transfer auto-encoder optimized by PSO *ISA Trans.* **105** 308–19
[12] Deng Z, Wang Z, Tang Z, Huang K and Zhu H 2021 A deep transfer learning method based on stacked autoencoder for cross-domain fault diagnosis *Appl. Math. Comput.* **408** 126318
[13] Li R, Li S, Xu K, Li X, Lu J and Zeng M 2022 A novel symmetric stacked autoencoder for adversarial domain adaptation under variable speed *IEEE Access* **10** 24678–89
[14] Jia M, Wang J, Zhang Z, Han B, Shi Z, Guo L and Zhao W 2022 A novel method for diagnosing bearing transfer faults based on a maximum mean discrepancies guided domain-adversarial mechanism *Meas. Sci. Technol.* **33** 015109
[15] Azamfar M, Singh J, Li X and Lee J 2021 Cross-domain gearbox diagnostics under variable working conditions with deep convolutional transfer learning *J. Vib. Control* **27** 854–64
[16] Wang X, Shen C, Xia M, Wang D, Zhu J and Zhu Z 2020 Multi-scale deep intra-class transfer learning for bearing fault diagnosis *Reliab. Eng. Syst. Saf.* **202** 107050
[17] Xia M, Shao H, Williams D, Lu S, Shu L and de Silva C W 2021 Intelligent fault diagnosis of machinery using digital twin-assisted deep transfer learning *Reliab. Eng. Syst. Saf.* **215** 107938
[18] Zeng M, Li S, Li R, Lu J, Xu K, Li X, Wang Y and Du J 2022 A hierarchical sparse discriminant autoencoder for bearing fault diagnosis *Appl. Sci.* **12** 818
[19] Zhang Q, Li H, Zhang X and Wang H 2021 Optimal multi-kernel local fisher discriminant analysis for feature dimensionality reduction and fault diagnosis *Proc. Inst. Mech. Eng.* O **235** 1041–56
[20] Tao X, Ren C, Li Q, Guo W, Liu R, He Q and Zou J 2021 Bearing defect diagnosis based on semi-supervised kernel local fisher discriminant analysis using pseudo labels *ISA Trans.* **110** 394–412
[21] Yin J and Yan X 2021 Stacked sparse autoencoders that preserve the local and global feature structures for fault detection *Trans. Inst. Meas. Control* **43** 3555–65
[22] Zhao X, Jia M and Liu Z 2021 Semisupervised deep sparse auto-encoder with local and nonlocal information for intelligent fault diagnosis of rotating machinery *IEEE Trans. Instrum. Meas.* **70** 3501413
[23] Tian Y, Tang Y and Peng X 2020 Cross-task fault diagnosis based on deep domain adaptation with local feature learning *IEEE Access* **8** 127546–59
[24] Wang T, Li T, Jiang P, Cheng Y, and Tang T 2022 A fault diagnosis method for rolling bearings based on inter-class repulsive force discriminant transfer learning *Meas. Sci. Technol.* **33** 095009
[25] Zou Y, Shi K, Liu Y, Ding G and Ding K 2021 Rolling bearing transfer fault diagnosis method based on adversarial variational autoencoder network *Meas. Sci. Technol.* **32** 115017
[26] Peng P, Zhang W, Zhang Y, Wang H and Zhang H 2022 Non-revisiting genetic cost-sensitive sparse autoencoder for imbalanced fault diagnosis *Appl. Soft Comput.* **114** 108138
[27] Qi Y, Shen C, Wang D, Shi J, Jiang X and Zhu Z 2017 Stacked sparse autoencoder-based deep network for fault diagnosis of rotating machinery *IEEE Access* **5** 15066–79
[28] Zhang J, Zhang Q, Qin X and Sun Y 2021 An intelligent fault diagnosis method based on domain adaptation for rolling bearings under variable load conditions *Proc. Inst. Mech. Eng.* C **235** 8025–38
[29] Qian W, Li S, Yao T and Xu K 2021 Discriminative feature-based adaptive distribution alignment (DFADA) for rotating machine fault diagnosis under variable working conditions *Appl. Soft Comput.* **99** 106886
[30] Wan L, Li Y, Chen K, Gong K and Li C 2022 A novel deep convolution multi-adversarial domain adaptation model for rolling bearing fault diagnosis *Measurement* **191** 110752
[31] Tang Z, Bo L, Liu X and Wei D 2021 An autoencoder with adaptive transfer learning for intelligent fault diagnosis of rotating machinery *Meas. Sci. Technol.* **32** 055110
[32] Li Y, Jiang W, Zhang G and Shu L 2021 Wind turbine fault diagnosis based on transfer learning and convolutional autoencoder with small-scale data *Renew. Energy* **171** 103–15
[33] Wen L, Gao L and Li X 2019 A new deep transfer learning based on sparse auto-encoder for fault diagnosis *IEEE Trans. Syst. Man Cybern. Syst.* **49** 136–44
[34] Sun M, Wang H, Liu P, Huang S, Wang P and Meng J 2022 Stack autoencoder transfer learning algorithm for bearing fault diagnosis based on class separation and domain fusion *IEEE Trans. Ind. Electron.* **69** 3047–58